Advancing Space Weather Forecasting: A Comparative Analysis of AI Techniques for Predicting Geomagnetic Storms

Shaimaa Salah
Department of Artificial Intelligence
Misr University For Science And Technology
Cairo, Egypt
98058@must.edu.eg

Asmaa ElSayed
Department of Artificial Intelligence
Misr University For Science And Technology
Cairo, Egypt
98047@must.edu.eg

Omar Khaled
Department of Artificial Intelligence
Misr University For Science And Technology
Cairo, Egypt
94105@must.edu.eg

Mohanad A.Deif
Department of Artificial Intelligence
Misr University For Science And Technology
Cairo, Egypt
Mohanad.Deif@must.edu.eg

Rania Elgohary
Department of Artificial Intelligence
Misr University For Science And Technology
Cairo, Egypt
Rania.elgohary@must.edu.eg

***Abstract*—Forecasting geomagnetic storms is crucial for mitigating their potential impacts on technology and infrastructure. This research explores the use of artificial intelligence (AI) techniques, particularly linear regression, and Long Short-Term Memory (LSTM) networks, for predicting geomagnetic storms using the OMNI dataset. The dataset, comprising various solar and interplanetary parameters, was preprocessed by scaling features and removing null values. A linear regression model achieved a Root Mean Squared Error (RMSE) of 5.95 and an R^2 score of 0.77. In contrast, the LSTM model, designed to capture temporal dependencies, significantly outperformed linear regression with an RMSE of 1.46 and an R^2 score of 0.99. These results demonstrate the potential of LSTM networks in accurately forecasting geomagnetic activity, thus providing a valuable tool for space weather prediction and the protection of critical technological systems.**

Keywords—Geomagnetic Storms; Forecasting; NASA; Deep learning; Machine learning; Artificial Intelligence.

I. INTRODUCTION

Geomagnetic storms, also known as space weather events, are large-scale disturbances in the Earth's magnetosphere caused by solar activity.[1] They originate from the Sun's dynamic and volatile environment, where solar flares, coronal mass ejections (CMEs), and high-speed solar wind streams interact with the Earth's magnetic field. These solar phenomena release vast amounts of energy and charged particles into space. When these particles collide with the Earth's magnetosphere, they induce currents and fields that can cause significant geomagnetic disturbances.[2]

The process begins with solar flares, which are sudden and intense bursts of radiation caused by the release of magnetic energy stored in the Sun's atmosphere.[3] These flares emit X-rays and ultraviolet radiation, which reach Earth within minutes, causing immediate but short-lived effects on the ionosphere. More impactful, however, are CMEs, which involve the ejection of billions of tons of plasma and magnetic field from the Sun's corona into space. [4] When these CMEs are directed towards Earth, they can take one to three days to arrive, carrying with them a powerful magnetic field. As this magnetic field interacts with Earth's own magnetic field, it can cause significant disruptions, leading to geomagnetic storms.[5]

One of the most notable historical examples of a geomagnetic storm is the Carrington Event of 1859, which remains the most powerful geomagnetic storm on record.[6] Named after the British astronomer Richard Carrington, who first observed the solar flare that triggered the event, the Carrington Event provides a dramatic illustration of the potential impact of geomagnetic storms. On September 1, 1859, Carrington observed a massive solar flare, followed by the arrival of a CME just 17 hours later. The geomagnetic storm that ensued was so intense that auroras were visible as far south as the Caribbean, and telegraph systems across North America and Europe failed, with some even catching fire due to induced currents. The event highlighted the vulnerability of electrical systems to space weather phenomena, even in the relatively nascent technological landscape of the 19th century.[7]

In today's highly interconnected and technologically dependent world, geomagnetic storms pose an even greater threat. Modern society relies heavily on a vast array of technologies that are susceptible to the effects of space weather. Satellites, which are critical for communication, navigation, and weather forecasting, can be damaged or rendered inoperative by the intense radiation and energetic particles associated with geomagnetic storms. Power grids are particularly vulnerable, as induced currents can overload transformers and other components, potentially leading to widespread blackouts.[8] High-frequency radio communications, used by aviation and maritime industries, can be disrupted, affecting navigation and safety. Additionally, geomagnetic storms can increase the drag on low-Earth orbit satellites, altering their trajectories and shortening their operational lifespans.Given these substantial risks, the ability to accurately predict and forecast geomagnetic storms is of paramount importance.[9] Traditional methods of forecasting rely on observational data from satellites and ground-based instruments, combined with empirical models to predict the arrival and impact of solar events. However, these methods have limitations in terms of accuracy and lead time. This is where artificial intelligence (AI) can play a transformative role.

AI techniques, particularly machine learning and deep learning, offer significant potential for improving the prediction of geomagnetic storms. By analyzing vast amounts of historical and real-time data, AI models can identify complex patterns and relationships that may not be apparent through traditional analysis. Machine learning algorithms, such as linear regression and support vector machines, can be used to predict the occurrence and intensity of geomagnetic storms based on solar wind parameters and other space weather data. More advanced techniques, like Long Short-Term Memory (LSTM) networks, are particularly well-suited for this task due to their ability to capture temporal dependencies and long-range correlations in sequential data.[10]

The use of AI in space weather forecasting has shown promising results. For instance, LSTM networks have been successfully applied to predict geomagnetic indices like the Kp index, which quantifies geomagnetic activity. These models have demonstrated the ability to provide more accurate and timely predictions compared to traditional methods, potentially giving operators of critical infrastructure more time to implement protective measures.[11]

Geomagnetic storms originate from dynamic solar activity and can have profound effects on modern technology. Historical events like the Carrington Event illustrate the potential severity of these storms. In today's technology-dependent world, accurate forecasting of geomagnetic storms is crucial, and AI techniques offer a powerful tool to enhance our predictive capabilities. By leveraging the strengths of AI, we can better prepare for and mitigate the impacts of geomagnetic storms, safeguarding our technological infrastructure and societal functions.

II. Related Works

This study [9] focuses on improving the evaluation of Deep Learning models for forecasting geomagnetic storms. While these models show promising results, traditional regression metrics like RMSE and R^2 don't adequately capture performance during high activity periods. To address this, the study introduces the Binned Forecasting Error, a metric tailored to assess model performance across different storm intensities. By standardizing datasets used for model training and testing, incorporating newer storm data, and considering various storm types, the study ensures fair model comparison. A comparative analysis between a neural network and a persistence model demonstrates the effectiveness of the new metric in evaluating forecasting performance, particularly during intense geomagnetic storms. Additionally, preliminary measurements from ACE are proposed to evaluate model performance in real-time settings, enhancing operational applicability.

This study [12] focuses on improving the accuracy of ionospheric Total Electron Content (TEC) modeling and forecasting, crucial for enhancing satellite navigation positioning accuracy. A NeuralProphet neural network model (NP) is developed, incorporating factors such as solar radiation flux index, geomagnetic activity index, geographic coordinates, and Global Ionospheric Map (GIM) data from the Chinese Academy of Sciences (CAS). The NP model is applied for short-term forecasting of ionospheric TEC over China during a severe magnetic storm in March 2015, and its performance is compared with a Long Short-Term Memory Neural Network (LSTM) model. Results show that the NP model outperforms the LSTM model, with lower root mean square error (RMSE) and relative deviation (RD) during the geomagnetic storm period. Additionally, the NP model demonstrates better accuracy across different latitudinal zones, indicating its effectiveness in characterizing spatial-temporal characteristics accurately under disturbed conditions over China.

This study [13] addresses a significant inconsistency in the treatment of the main phase (MP) of geomagnetic storms, particularly in the early decreasing part from the positive main phase onset (MPO) to the 0-level of Dst and SymH indices. By correcting this inconsistency in 848 storms with positive MPO out of 1164 storms during 1981–2019, the study raises the 0-level of SymH to the MPO-level. This correction, which considers the full range of the main phase, leads to increases in the corrected storm intensity (SymHMin*) and impulsive strength (IpsSymH*) by up to -149 nT and -134 nT, respectively. These corrections have significant implications for global space weather, affecting storm identification, classification, and the ability to distinguish severe space weather (SvSW) events from normal space weather (NSW) events. Additionally, the corrected IpsSymH* effectively identifies minor-system-damage space weather (MSW) events from NSW events.

This [14] study explores the prediction of geomagnetic disturbances using machine learning techniques, focusing on the Long-Short Term Memory (LSTM) recurrent neural network. Utilizing in-situ measurements of solar wind plasma and magnetic field data collected over multiple solar cycles from 2005 to 2019 at the Lagrangian point L1, the study employs binary classification to forecast a decrease in the SYM-H geomagnetic activity index below the threshold of -50 nT, indicative of magnetospheric perturbations, one hour in advance. Addressing the strong class imbalance issue, the study utilizes an appropriate loss function tailored to optimize skill scores during training. Additionally, value-weighted skill scores are employed to evaluate predictions, considering the strong temporal variability of the problem. For the first time, the study incorporates the content of magnetic helicity and energy carried by solar transients as input features in the neural network architecture, demonstrating their predictive capabilities through correlation-driven feature selection. The study showcases the optimal performance of the LSTM neural network in accurately forecasting the onset of geomagnetic storms, a critical aspect for providing real-time warnings in operational settings.

This paper [15] provides a comprehensive review of the authors' research spanning the past decade concerning the identification and forecasting of severe space weather (SvSW). SvSW events are distinguished by their capacity to cause significant damage to ground installations, such as transformers and telecommunication networks, while normal space weather (NSW) does not result in such severe effects. The study highlights that very energetic coronal mass ejections (CMEs), particularly characterized by sharp changes at their leading edge or front, are the primary cause

of SvSW events. The research identifies specific parameters, including the interplanetary CME (ICME) front's velocity jump and the magnitude of the southward interplanetary magnetic field (IMF Bz) at and beyond this velocity jump, as crucial factors in causing SvSW. Additionally, the study introduces the impulsive strength (IpsDst) parameter, derived from the average value of Dst during the storm main phase (MP), as a means to distinguish between SvSW and NSW. Furthermore, it proposes a novel forecasting approach based on the product of the observed velocity jump and associated IMF Bz southward (ΔVBz), enabling the prediction of SvSW events with an advance warning time of approximately half an hour, provided estimates of ΔVBz at the Sun-Earth L1 point are available, possibly derived from observations such as those from the Advanced Composition Explorer (ACE) satellite.

This study [16] explores the challenging task of forecasting geomagnetic activity, which exhibits nonlinear variability characterized by heavy-tailed probability distributions and intermittent outliers. Given the potential threats posed by geomagnetic storms to satellites and power grids, there is significant interest in predicting outlier events. The proposed model combines neural networks and regressions trained over moving windows of observations to adapt to new data. Logistic regression is employed to predict periods of high activity, utilizing the cumulative distribution function as a causal input in time series and machine learning models. Using the Aa index dataset, corrected for secular drift, forecasting experiments are conducted over horizons ranging from 1 to 4 days. Comparative analyses with other models, including time-varying parameter regressions and a recurrent neural network with fixed weights, demonstrate that the model combining neural net and logistic regression achieves the most accurate forecasts, followed closely by regression alone. The study highlights the trade-off between prediction accuracy and the ability to forecast outliers, influenced by the width of the moving window. Wider windows yield lower overall errors but miss outliers, while narrower windows better predict outliers but may call them at incorrect times, resulting in higher average errors. Additionally, while the model achieves greater accuracy at shorter horizons, its performance deteriorates rapidly over longer forecasting horizons.

III. DATASET

The dataset used in this research is derived from the OMNI (Operational Magnetic and Ionospheric Data) dataset, which is provided by NASA.[17] This dataset compiles a wide range of solar wind, magnetic field, and other space weather parameters, which are essential for understanding and forecasting geomagnetic storms. The OMNI dataset is particularly valuable due to its comprehensive nature and its historical depth, providing continuous data from multiple sources, including satellites and ground-based observations.

3.1. Data Preprocessing

Before delving into the specifics of the dataset, it's important to understand the preprocessing steps that were applied to ensure the data's suitability for analysis:

3.1.1. Reading and Cleaning the Data:

The dataset was loaded from a CSV file, which included an initial column named Unnamed: 0 that was dropped as it was unnecessary for analysis.
Columns representing Year, Day, and Hour were combined to create a single date column, enabling time-series analysis.

3.1.2. Handling Missing Values:

Any rows with missing values were removed to ensure the integrity of the dataset and to facilitate accurate modeling.

3.1.3. Sorting and Resetting Index:

The dataset was sorted by the date column, and the index was reset to maintain a clean and sequential ordering of data points.

The final dataset after preprocessing consists of 50 features, which can be grouped into several categories:

Time-related Columns:

- date: A datetime column representing the exact timestamp for each recorded observation.
- Solar Wind and Magnetic Field Parameters
- Field Magnitude Avg: The average magnitude of the interplanetary magnetic field (IMF).
- Magnitude of Average Field vector: The average magnitude of the IMF vector.
- Lat. Angle of avg. Field vector: The latitude angle of the average IMF vector.
- Long. Angle of avg. Field vector: The longitude angle of the average IMF vector.
- Bx,GSE, By,GSE, Bz,GSE: Components of the IMF in the Geocentric Solar Ecliptic (GSE) coordinate system.
- By,GSM, Bz,GSM: Components of the IMF in the Geocentric Solar Magnetospheric (GSM) coordinate system.

Solar Wind Plasma Parameters:

- Proton temperature: The temperature of protons in the solar wind.
- Proton density: The density of protons in the solar wind.
- Bulk speed: The speed of the solar wind.
- Bulk flow longitude, Bulk flow latitude: The direction of the solar wind flow.
- Na/Np: The ratio of alpha particles to protons.
- Flow Pressure: The dynamic pressure of the solar wind.

Standard Deviation Measures:

- Sigma-|B|, Sigma-B, Sigma-Bx, Sigma-By, Sigma-Bz: Standard deviations of the magnetic field components and magnitude.
- Sigma-T, Sigma-n, Sigma-V, Sigma-phi-V, Sigma-theta-V: Standard deviations of temperature, density, velocity, and flow angles.

Energetic Particle Fluxes:

- PROT Flux >1 MeV, PROT Flux >2 MeV, PROT Flux >4 MeV, PROT Flux >10 MeV, PROT Flux

>30 MeV, PROT Flux >60 MeV: Fluxes of protons at different energy levels.

Geomagnetic Indices and Other Parameters:

- Kp*10: A measure of geomagnetic activity, multiplied by 10 to transform it into a more manageable range.
- R: The sunspot number, indicating solar activity.
- DST Index: The disturbance storm time index, representing the strength of the ring current around Earth.
- AE-index: The auroral electrojet index, indicating auroral activity.
- M'SPH Flux Flag: A flag indicating the flux of energetic particles in the magnetosphere.
- Ap-index: A daily index of geomagnetic activity.
- f10.7_index: The solar radio flux at 10.7 cm wavelength, an indicator of solar activity.
- PC(N): The polar cap index, indicating geomagnetic activity in the polar regions.
- AL-index, AU-index: Indices representing the auroral lower and upper activity levels.
- MAC: A miscellaneous column related to magnetic activity.

3.1.4. Data Scaling and Splitting:

To prepare the data for machine learning models, the following steps were taken:

Scaling:

The features were scaled using the MinMaxScaler to normalize the values between 0 and 1, ensuring that all features contribute equally to the model.

Splitting:

The dataset was split into training and test sets in an 80-20 ratio. This chronological split ensured that the model was trained on past data and tested on future data, simulating a real-world forecasting scenario.

Reshaping for LSTM:

For the LSTM model, the input data was reshaped into a three-dimensional array with the structure [samples, timesteps, features].

Target Variable:

- Kp*10: This is the target variable for prediction, representing the geomagnetic activity index scaled by a factor of 10. It provides a quantifiable measure of the intensity of geomagnetic storms.

This extensive dataset, with its diverse range of solar and geomagnetic parameters, provides a robust foundation for developing and testing AI models aimed at forecasting geomagnetic storms. By leveraging these comprehensive features, the models can learn to predict geomagnetic activity with high accuracy, thereby contributing to better preparedness and mitigation strategies for space weather impacts.

IV. METHODOLOGY

This section outlines the methodology employed in this research, detailing the development, training, and evaluation of the AI models used for forecasting geomagnetic storms. The focus is on the selection of models, the principles behind them, training procedures, and the evaluation metrics used to measure their performance.

4.1. Model Selection

Two primary models were selected for this research: Linear Regression and Long Short-Term Memory (LSTM) networks. These models were chosen to explore both traditional and advanced AI techniques for forecasting geomagnetic storms.

4.1.1. Linear Regression

Linear Regression is a fundamental statistical method that assumes a linear relationship between the independent variables (features) and the dependent variable (target). The primary objective of Linear Regression is to model the relationship between the features and the target by fitting a linear equation to observed data. The Linear Regression model can be mathematically represented as follows:

$$\hat{y} = \beta 0 + \beta 1 x1 + \beta 2 x2 + \cdots + \beta n xn \quad (1)$$

Where:

- $\hat{y}$ is the predicted value.
- $\beta 0$ is the intercept of the regression line.
- $\beta 1, \beta 2, \ldots\ldots, \beta n$ are the coefficients for the independent variables $x1, x2, \ldots\ldots, xn$.

The model parameters $\beta 1, \beta 2, \ldots\ldots, \beta n$ are estimated using the least squares method, which minimizes the sum of the squared differences between the observed values and the predicted values.

4.1.2. Long Short-Term Memory (LSTM) Networks:

LSTM networks are a type of Recurrent Neural Network (RNN) designed to capture long-term dependencies in sequential data. They are particularly suited for time-series forecasting due to their ability to retain information over long periods. The core component of an LSTM network is the LSTM cell, which consists of three main gates: the forget gate, the input gate, and the output gate. These gates control the flow of information and help the network manage its memory.

The key equations for an LSTM cell are as follows:

The forget gate is responsible for deciding which information from the previous cell state should be discarded. It takes the previous hidden state (h_{t-1}) and the current input (x_t), combining them and passing the result through a sigmoid activation function. The sigmoid function outputs values between 0 and 1, where a value closer to 0 means "completely forget" and a value closer to 1 means "completely retain." This mechanism helps the network decide the proportion of the previous cell state to be kept in the current state.

$$f_t = \sigma\left(W_f \times [h_{t-1}, x_t] + B_f\right) \quad (2)$$

The input gate controls how much new information is added to the cell state. It operates in two stages. First, it creates a candidate cell state ($\tilde{c}_t$) by applying a tanh activation function to the combined previous hidden state and current input. This candidate represents new information that could

potentially be added to the cell state. Second, the input gate uses a sigmoid activation function to decide which parts of this candidate cell state should be updated. The combination of these outputs determines the new cell state.

$$i_t = \sigma(W_i \times [h_{t-1}, x_t] + B_i) \quad (3)$$

$$\tilde{c}_t = tanh\,(W_c \times [h_{t-1}, x_t] + B_c) \quad (4)$$

The output gate decides the output of the LSTM cell, which also influences the hidden state. This gate takes the previous hidden state and the current input, passes them through a sigmoid activation function to determine the relevant parts of the cell state that should be output. This result is then multiplied by the tanh of the current cell state to produce the new hidden state, effectively determining what information should be carried forward to the next time step.

$$O_t = \sigma(W_o \times [h_{t-1}, x_t] + B_o) \quad (5)$$

$$c_t = f_t \times c_{t-1} + i_t \circ \tilde{c}_t \quad (6)$$

$$h_t = o_t \times tanh\,(c_t) \quad (7)$$

LSTMs are effective in learning from the sequential patterns in the data, which makes them suitable for time-series forecasting tasks such as predicting geomagnetic activity.

4.2. Model Training

4.2.1. Linear Regression

The Linear Regression model was trained using scaled training data. The goal during training was to find the optimal values for the model parameters $\beta 1, \beta 2, \ldots\ldots, \beta n$ by minimizing the mean squared error (MSE) between the predicted and actual values of the target variable KP*10,
The model fitting process involves solving the normal equations or using gradient descent algorithms to iteratively update the model parameters until the error is minimized.

4.2.2. Long Short-Term Memory (LSTM) Networks

The LSTM model was constructed with an input layer, one LSTM layer containing 50 units, and a dense output layer. The LSTM layer captures the temporal dependencies in the data, while the dense layer maps the LSTM outputs to the prediction of KP*10.
The model was compiled with Mean Absolute Error (MAE) as the loss function and the Adam optimizer. MAE was chosen for its robustness to outliers, and the Adam optimizer was selected for its efficiency and ability to handle large datasets. The training process involved feeding the scaled and reshaped training data into the model in mini-batches and adjusting the weights through backpropagation through time (BPTT).

To prevent overfitting, early stopping was implemented during training. This technique monitors the validation loss and stops the training process when the validation loss ceases to improve, ensuring that the model generalizes well to unseen data.

4.3. Evaluation Metrics

The performance of both models was assessed using two primary metrics: Root Mean Squared Error (RMSE) and R^2 score. These metrics provide a comprehensive evaluation of the models' predictive capabilities.

4.3.1. Root Mean Squared Error (RMSE):

RMSE is defined as the square root of the average squared differences between the predicted and actual values. It provides a measure of the model's prediction accuracy, with lower values indicating better performance. The formula for RMSE is:

$$RMSE = \sqrt{\frac{1}{n}\Sigma_{i=1}^{n}\left(\frac{d_i - f_i}{\sigma_i}\right)^2} \quad (8)$$

where n is the number of data points.

4.3.2. R^2 Score (Coefficient of Determination):

The R^2 score represents the proportion of the variance in the target variable that is predictable from the input features. It ranges from 0 to 1, with higher values indicating better model performance. The formula for R^2 score is:

$$SS_{res} = \sum_i (y_i - f_i)^2 = \sum_i e_i^2 \quad (9)$$

$$SS_{total} = \sum_i (y_i - \bar{y})^2 \quad (10)$$

$$y = \frac{1}{n}\sum_{i=1}^{n} y_i, \quad (11)$$

$$R^2 = 1 - \frac{SS_{res}}{SS_{total}} \quad (12)$$

The RMSE metric provides insight into the average prediction error, while the R^2 score indicates the proportion of variability explained by the model. Together, these metrics offer a comprehensive view of the model's performance.

4.4. Results Visualization

To provide a comprehensive evaluation of the models' performances, actual vs. predicted values were plotted for both Linear Regression and LSTM models. These visualizations help in understanding how closely the models' predictions match the actual geomagnetic activity over time.

In conclusion, the methodology section details the careful selection and training of both a traditional Linear Regression model and an advanced LSTM network to forecast geomagnetic storms. By using robust evaluation metrics and visualization techniques, this research ensures a thorough assessment of the models' predictive capabilities, contributing to the advancement of AI techniques in space weather forecasting.

V. RESULTS

This section presents the results obtained from the Linear Regression and Long Short-Term Memory (LSTM) models for forecasting geomagnetic storms. The performance of both models was evaluated using the Root Mean Squared Error (RMSE) and R^2 score, and the results were visualized

to provide a clear comparison between the predicted and actual values.

5.1. Linear Regression Model Results

5.1.1. Model Performance

The Linear Regression model was trained on 80% of the dataset and tested on the remaining 20%. The performance of the model was measured using RMSE and R^2 score on the test data.

- Root Mean Squared Error (RMSE): The RMSE of the Linear Regression model on the test set was found to be 5.946. This indicates that, on average, the model's predictions deviate from the actual values by approximately 5.946 units of the Kp*10 index.

- R^2 Score: The R^2 score for the Linear Regression model was 0.771. This means that the model explains 77.1% of the variance in the Kp*10 index, suggesting a relatively good fit considering the simplicity of the model.

5.1.2. Visualizing Predictions

The actual vs. predicted values for the Linear Regression model are plotted to visualize the model's performance. The plot reveals how closely the predicted values track the actual geomagnetic activity over the test period. While there is a general alignment between the two, some deviations indicate areas where the model could improve.

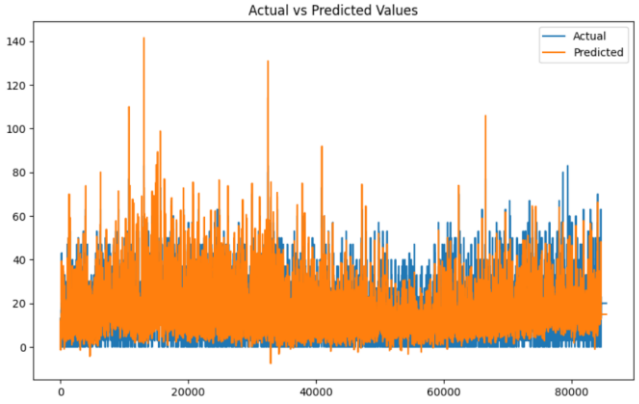

Figure 1: Actual vs Predicted linear regression Results.

5.1.3. Analysis

The Linear Regression model provides a straightforward baseline for forecasting geomagnetic storms. Although it performs reasonably well with an R^2 score of 0.771, the RMSE value suggests that the predictions could be refined further. The linear nature of this model limits its ability to capture complex patterns and dependencies in the data, highlighting the need for more sophisticated models.

5.2. Long Short-Term Memory (LSTM) Model Results

Model Performance

The LSTM model was also trained on 80% of the dataset and evaluated on the remaining 20%. The performance metrics for the LSTM model are significantly better than those for the Linear Regression model.

- Root Mean Squared Error (RMSE): The RMSE of the LSTM model on the test set was 1.461. This lower RMSE value indicates that the LSTM model's predictions are much closer to the actual values compared to the Linear Regression model.

- R^2 Score: The R^2 score for the LSTM model was 0.986. This high R^2 value indicates that the LSTM model explains 98.6% of the variance in the Kp*10 index, demonstrating its superior ability to capture the underlying patterns in the data.

5.2.1. Visualizing Predictions

The actual vs. predicted values for the LSTM model were plotted to provide a visual comparison. The plot shows that the LSTM model's predictions closely follow the actual geomagnetic activity, with minimal deviations. This visual confirmation underscores the effectiveness of the LSTM model in forecasting geomagnetic storms.

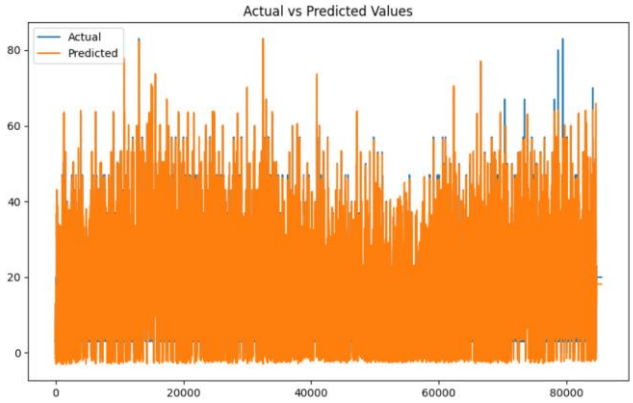

Figure 2: Actual vs Predicted LSTM Results.

5.2.2. Analysis

The LSTM model significantly outperforms the Linear Regression model, as evidenced by its lower RMSE and higher R^2 score. The ability of LSTM networks to capture long-term dependencies and sequential patterns in the data is evident from these results. The LSTM model's performance indicates that it can effectively learn and predict the complex temporal dynamics associated with geomagnetic activity.

5.3. Comparative Analysis

A comparative analysis of the two models highlights the advantages of using advanced AI techniques like LSTM networks for time-series forecasting. While the Linear Regression model provides a good starting point, its linear assumptions limit its predictive accuracy. In contrast, the LSTM model's capacity to learn from sequential data and capture intricate patterns makes it a superior choice for this task.

RMSE Comparison: The RMSE for the Linear Regression model (5.946) is significantly higher than that for the LSTM model (1.461), indicating that the LSTM model's predictions are much closer to the actual values.

R^2 Score Comparison: The R^2 score for the Linear Regression model (0.771) is lower than that for the LSTM

model (0.986), suggesting that the LSTM model accounts for a much larger proportion of the variance in the target variable.

VI. Conclusion

This research underscores the significance of leveraging advanced AI techniques, particularly LSTM networks, for forecasting geomagnetic storms, as demonstrated through comparative analysis with a traditional Linear Regression model. While Linear Regression provided a foundational understanding, the LSTM network's superior performance, with significantly lower RMSE and higher R^2 score, highlights its efficacy in capturing complex temporal dynamics inherent in space weather data. These findings underscore the critical role of AI in enhancing the accuracy of geomagnetic storm forecasts, crucial for safeguarding modern technology and infrastructure. Moving forward, further advancements in model architectures, feature engineering, and real-time forecasting capabilities promise to enhance the practical applicability and reliability of AI-driven space weather prediction systems, ultimately mitigating the adverse impacts of geomagnetic storms on society and industry.

Acknowledgment

We would like to express our sincere gratitude to NASA for providing access to the OMNI dataset, which served as the foundation for this research. We extend our appreciation to all the researchers and scientists whose contributions to the field of space weather forecasting have paved the way for advancements in predictive modeling. Additionally, we acknowledge the support and guidance provided by our academic advisors and colleagues throughout the course of this study. Their valuable insights and encouragement have been instrumental in shaping this research.

References

[1] U. Aksen, Ü. D. Göker, E. Timoçin, Ç. Akçay, and M. İpek, "The effect of geomagnetic storms on aircraft accidents between the years 1919–2023 in civil aviation," *Adv. Sp. Res.*, vol. 73, no. 1, pp. 807–830, 2024, doi: https://doi.org/10.1016/j.asr.2023.11.008.

[2] C. Wang, Q. Ye, F. He, B. Chen, and X. Zhang, "A New Method for Predicting Non-Recurrent Geomagnetic Storms," *Sp. Weather*, vol. 21, no. 8, p. e2023SW003522, 2023.

[3] S. Nitti, T. Podladchikova, S. J. Hofmeister, A. M. Veronig, G. Verbanac, and M. Bandić, "Geomagnetic storm forecasting from solar coronal holes," *Mon. Not. R. Astron. Soc.*, vol. 519, no. 2, pp. 3182–3193, 2023, doi: 10.1093/mnras/stac3533.

[4] F. Basciftci, "Using artificial neural networks in the investigation of four moderate geomagnetic storms (mGSs) that occurred in 2015," *Adv. Sp. Res.*, vol. 71, no. 10, pp. 4382–4400, 2023, doi: https://doi.org/10.1016/j.asr.2023.01.001.

[5] S. Bianco *et al.*, "Prediction of Adverse effects of Geomagnetic storms and Energetic Radiation (PAGER)," *EGUGA*, p. EGU-8128, 2023, doi: 10.5194/EGUSPHERE-EGU23-8128.

[6] E. C. McGinness, T. J. Immel, B. J. Harding, Y. J. Wu, and C. C. Triplett, "The Effects of a Small Geomagnetic Storm on Earth's Thermosphere and Ionosphere: ICON Observations of the 25 January 2021 Disturbance," *J. Geophys. Res. Sp. Phys.*, vol. 128, no. 7, p. e2022JA031207, Jul. 2023, doi: 10.1029/2022JA031207.

[7] M. S. Pulinets, P. A. Budnikov, and S. A. Pulinets, "Global Ionospheric Response to Intense Variations of Solar and Geomagnetic Activity According to the Data of the GNSS Global Networks of Navigation Receivers," *Geomagn. Aeron.*, vol. 63, no. 2, pp. 172–185, 2023, doi: 10.1134/S0016793222600898.

[8] D. Telloni *et al.*, "Prediction Capability of Geomagnetic Events from Solar Wind Data Using Neural Networks," *Astrophys. J.*, vol. 952, no. 2, p. 111, 2023, doi: 10.3847/1538-4357/acdeea.

[9] A. Collado-Villaverde, P. Muñoz, and C. Cid, "A Framework for Evaluating Geomagnetic Indices Forecasting Models," *Sp. Weather*, vol. 22, no. 3, p. e2024SW003868, 2024, doi: https://doi.org/10.1029/2024SW003868.

[10] W. Xu *et al.*, "A class of Bayesian machine learning model for forecasting Dst during intense geomagnetic storms," *Adv. Sp. Res.*, vol. 72, no. 9, pp. 3882–3889, 2023, doi: https://doi.org/10.1016/j.asr.2023.07.009.

[11] T. Gulyaeva, M. Hernández-Pajares, and I. Stanislawska, "Ionospheric Weather at Two Starlink Launches during Two-Phase Geomagnetic Storms," *Sensors*, vol. 23, no. 15, p. 7005, 2023.

[12] M. A. Bin *et al.*, "Study on the NeuralProphet forecast TEC model over China during the severe geomagnetic storm in March 2015," *Chinese J. Geophys. (in Chinese)VL - 67*, no. 2, pp. 452–460, 2024, doi: 10.6038/cjg2023R0225.

[13] V. Manu, N. Balan, Y. Ebihara, Q.-H. Zhang, and Z.-Y. Xing, "A fresh look at the intensity and impulsive strength of geomagnetic storms," *Geosci. Lett.*, vol. 11, no. 1, p. 22, 2024, doi: 10.1186/s40562-024-00337-7.

[14] S. Guastavino *et al.*, "Forecasting Geoffective Events from Solar Wind Data and Evaluating the Most Predictive Features through Machine Learning Approaches." 2024.

[15] N. Balan, Q.-H. Zhang, S. T. Ram, K. Shiokawa, V. Manu, and Z.-Y. Xing, "How to identify and forecast severe space weather events," *J. Atmos. Solar-Terrestrial Phys.*, vol. 256, p. 106183, 2024, doi: https://doi.org/10.1016/j.jastp.2024.106183.

[16] G. Reikard, "Forecasting geomagnetic activity: Neural networks, moving windows and state transition models," *J. Atmos. Solar-Terrestrial Phys.*, vol. 256, p. 106201, 2024, doi: https://doi.org/10.1016/j.jastp.2024.106201.

[17] National Aeronautics and Space Administration (NASA), "NASA OMNI Dataset." [Online]. Available:https://omniweb.gsfc.nasa.gov/form/dx1.ht